

# Optimal Energy Management for Stable Operation of an Islanded Microgrid

Luis I. Minchala-Avila<sup>1</sup>, *Member, IEEE*, Luis Garza-Castañón<sup>2</sup>, *Member, IEEE*, Youmin Zhang<sup>3</sup>, *Senior Member, IEEE*, and Héctor J. Altuve Ferrer<sup>4</sup>, *Fellow, IEEE*.

**Abstract**—This paper presents a methodology on the design of an optimal predictive control scheme applied to an islanded microgrid. The controller manages the batteries energy and performs a centralized load shedding strategy to balance the load and generation within the microgrid, and to keep the stability of the voltage magnitude. A nonlinear model predictive control (NMPC) algorithm is used for processing a data set composed by the batteries state of charge (SOC), the distributed energy resources (DERs) active power generation, and the forecasted load. The NMPC identifies upcoming active power unbalances and initiates automated load shedding over non-critical loads. The control strategy is tested in a medium voltage distribution system with DERs. This control strategy is assisted by a distribution monitoring system (DMS), which performs real-time monitoring of the active power generated by the DERs and the current load demand at each node of the microgrid. Significant performance improvement is achieved with the use of this control strategy over tested cases without its use. The balance between the power generated by the DERs and the load demand is maintained, while the voltage magnitude is kept within the maximum variation margin of  $\pm 5\%$  recommended by the standard ANSI C84.1-1989.

**Index Terms**—Energy management, load shedding, microgrid control

## I. INTRODUCTION

Electric power systems have evolved over more than a century from isolated networks to interconnected grids that generate, transmit, and distribute electric energy over large geographical areas. The worldwide search for green power generation resources has fostered the development of wind, solar, and other types of generation sources, which are being connected in distribution and subtransmission networks [1].

The topology of today's radial distribution networks is fixed and suffers changes only after the occurrence of a fault, since networks were planned for unidirectional power flow. Many distribution networks were not originally conceived to handle bidirectional power flows, therefore changes are needed in the way they are designed, operated and controlled. For instance,

Copyright (c) 2016 IEEE. Personal use of this material is permitted. However, permission to use this material for any other purposes must be obtained from the IEEE by sending a request to [pubs-permissions@ieee.org](mailto:pubs-permissions@ieee.org)

<sup>1</sup> Universidad de Cuenca, Av. 12 de Abril, Cuenca, Ecuador

<sup>2</sup> Tecnológico de Monterrey, Eugenio Garza Sada 2501, Monterrey NL, México

<sup>3</sup> Xi'an University of Technology, Xi'an, Shaanxi, China, and Concordia University, 1455 de Maisonneuve W., Montreal QC, Canada (Corresponding author, currently on sabbatical leave from Concordia University; Email: [yumin.zhang@xaut.edu.cn](mailto:yumin.zhang@xaut.edu.cn); [yumin.zhang@concordia.ca](mailto:yumin.zhang@concordia.ca)); The author's work was financially supported in part by NSERC, NSFC #61573282 and SPNSF #2015JZ020.

<sup>4</sup> Schweitzer Engineering Laboratories, Inc.

Kabir *et al.* [2] propose a coordinated control of photovoltaic (PV) array units and battery storage systems (BSS) for voltage control of a residential distribution system.

Several contributions on control strategies of microgrids have been made. Planas *et al.* [3] provide details about the control tasks involved in the microgrids management with a review on the main types of controls proposed in the literature. Reference [4] details an energy management system (EMS) of a grid-connected microgrid. The microgrid is composed of a wind turbine (WT), a PV array and an energy storage system (ESS). A two-level control architecture based on an adaptive neuro-fuzzy inference system (ANFIS) is proposed. The ANFIS-based supervisory control determines the power that must be delivered by/stored in the ESS. The lowest control level controls the converters associated with the renewable energy sources (RES) and ESS.

Reference [5] describes a power grid solution, which consists of a decentralized power system with a two-level control architecture that coordinates power-flows generated by the DERs within a microgrid. Reference [6] describes a central controller for microgrids, which optimizes the microgrid operation when it is connected to the main power system. Similar approaches of centralized microgrid controllers are presented in [7]. Distributed control strategies for the two operation modes of a microgrid: grid-connected and islanded, with different techniques are studied in [8]–[10]. A review of optimal control techniques applied to EMS for microgrids is presented in [11]. The majority of contributions on the design of an EMS consider a favorable scenario during the microgrid operation, where  $P_{gen} > P_{load}$ . This paper addresses the important issue, when circumstantially  $P_{gen}$  could be lower than  $P_{load}$ . A predictive algorithm is a natural choice for handling these problems.

This research work is aimed at developing an EMS for isolated power distribution systems that integrate DERs. The EMS performs automated load shedding of non-critical loads when foreseeable power unbalances could affect the stability of the microgrid. The voltage magnitude of the network is kept within safe limits. An NMPC algorithm is proposed to process a data set composed by the batteries SOC, current DERs power generation and the forecasted load for identifying upcoming generation problems when the microgrid is operating in islanded mode, in order to execute the corresponding control actions. The NMPC algorithm is selected mainly due to its capabilities on prediction, and constraints management in the states and control signals. Two microgrid models for computing the control actions within the NMPC strategy are used:

1) power-flow calculation through the Newton-Raphson (NR) algorithm with a load predictor implemented with artificial neural networks (ANNs), and 2) an autoregressive model with external input (ARX) obtained through a data-based modeling approach using ANFIS. This control strategy is assisted by a DMS, which performs real-time monitoring of the power generated by the DERs and the actual load demand at each microgrid node.

This paper is organized as follows: Section II presents a description on the microgrid under study. Section III details the controller design. Section IV shows simulation results. Section V presents the conclusions.

## II. SCENARIO DESCRIPTION

### A. Microgrid Benchmark Model Overview

Operating characteristics of a microgrid are different from those of a bulk power system: smaller generation inertia, variable power generation due to RES integration, low fault currents when islanded, etc.. This fact supports the idea of building a detailed simulation platform for investigating the behavior of such networks. References [12]–[14] present benchmark models of medium and low voltage distribution networks with DG. The benchmark models are analyzed in different operating conditions with and without the inclusion of storage systems, although no optimal control techniques are proposed for managing loads and batteries to ensure a reliable microgrid islanded operation. This paper addresses this important topic.

Stable operation of an electric power system requires the voltage magnitude to be kept within a range of about  $\pm 5\%$  of the nominal value. Standard IEEE 1547.2-2008 [15] states that for interconnecting distributed resources with electric power systems, the total time should be less than 0.15 seconds when the frequency variation exceeds 0.5 Hz and the voltage variation exceeds 5% of its nominal value. It is a challenging task to integrate DERs into a distribution network and to operate this network (microgrid) within the limits of the established operation standards. Therefore, first step for developing an integration framework is to have a testing platform. The medium voltage benchmark model presented in [12], [16] with some modifications, detailed in Subsection II.B, will be used for this purpose. Fig. 1 shows such a microgrid configuration.

A detailed guide of recommendations about the operation of islanded microgrids is presented in the Standard IEEE 1547.4-2011 [17]. The control strategy must ensure that critical loads receive service priority when the microgrid operates in isolated mode. Islanding operation could be planned or could be the result of emergency conditions. For example, a fault or disturbance can cause tripping of breakers resulting in an intentional island. When islanding occurs in a distribution network, voltage and frequency are severely disturbed due to imbalance between generation and load demand. During islanded operation, the DERs must be able to carry the load on the islanded section and to guarantee a safe and stable microgrid operation within certain voltage and frequency limits. When the available power generation capacity is smaller than load demand, load shedding is needed to restore the balance.

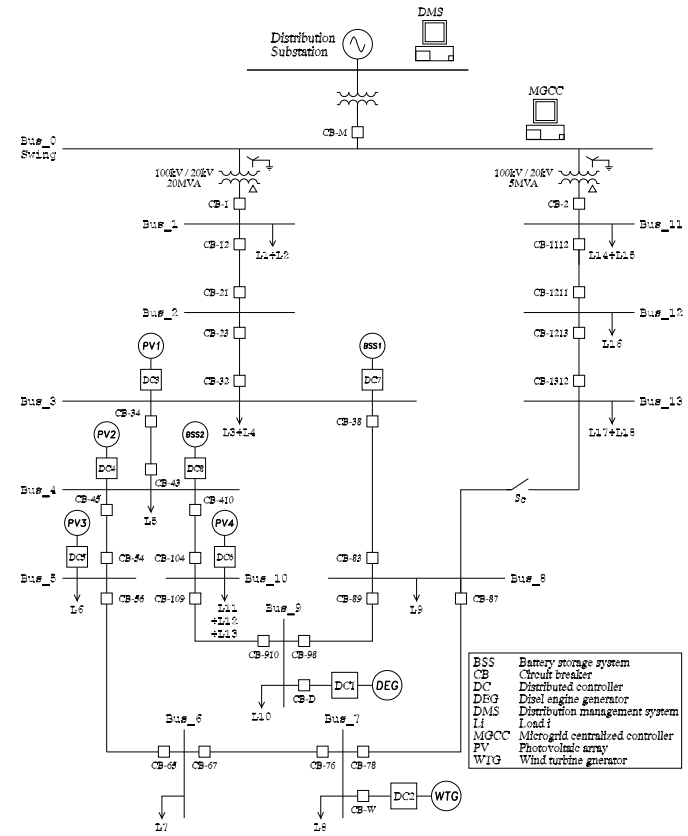


Fig. 1. Medium voltage microgrid benchmark model

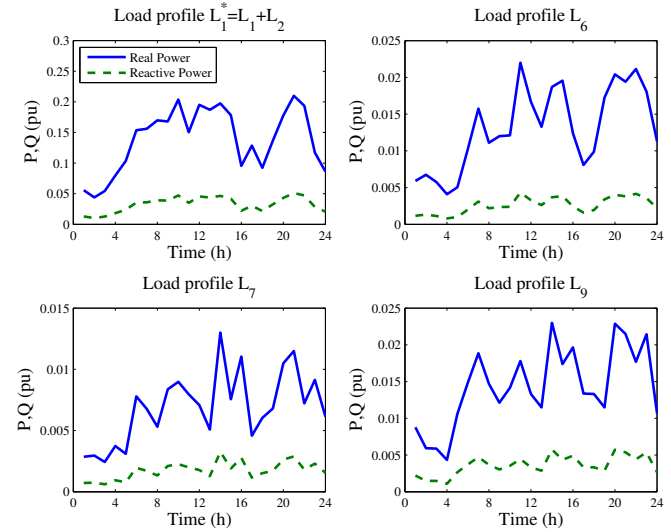


Fig. 2. Load profiles

### B. Main Characteristics of the Benchmark Model

Fig. 1 shows the microgrid benchmark model configuration developed throughout this research, which consists of two feeders supplied by a distribution substation. A grid of DERs is connected to the left side feeder, including four PV array units, one wind turbine generator (WTG), two BSS, and one diesel

engine generator (DEG). Each DER has a distributed controller (DC). The microgrid benchmark model is implemented in the SimPowerSystems of Simulink.

The rated voltage level of the network is 20 kV. It is supplied from two 5 MVA, 110/20 kV transformers. The network includes underground and overhead lines. The network parameters and loads characteristics were taken from [16] and are summarized in Tables II and III in the Appendix. Although maximum values for active and reactive power loads are considered, variable load profiles have been generated for loads  $L_1, L_2, L_6, L_7$  and  $L_9$ . Homer Energy was used for this purpose, taking as base values:  $S_{base} = 5 \text{ MW}$  and  $V_{base} = 20 \text{ kV}$ . Fig. 2 shows the load profiles.

The DERs, whose modeling details for control purposes have been presented in previous research papers [18]–[20], have the following characteristics:

- **DEG:** A diesel engine (DE) is used as the prime mover of a synchronous generator. In an islanded configuration, the system frequency is determined by the DE mechanical speed  $\omega_m$ , while the synchronous generator field current sets the voltage magnitude. The maximum output power of the DEG is 1.5625 MVA (0.3125 pu). The excitation voltage of the synchronous generator is regulated for maintaining the terminal voltage constant (voltage control mode). For this mode, the synchronous machine is considered as a voltage controlled bus in the power flow calculation.
- **WTG:** A horizontal-axis WT has been chosen as the prime mover of an induction generator. The WT model selected has a lumped mass, with pitch control through the variation of blade pitch angle,  $\beta$ . The maximum output power of the WTG is 1 MVA (0.2 pu).
- **PV array:** 330 SunPower modules (SPR-305) are used. In the particular case of PV<sub>1</sub>, the array consists of 66 strings of 5 series-connected modules connected in parallel ( $66 \times 5 \times 305.2 \frac{\text{W}}{\text{module}} = 100.7 \text{ kW}$ ), or 0.02 pu. PV<sub>2</sub>, PV<sub>3</sub> and PV<sub>4</sub> have  $0.02, 4 \times 10^{-3}$  and  $5 \times 10^{-3}$  pu of power generation capacity, respectively. The boost converter and voltage source converter (VSC) of the PV array are represented by equivalent voltage sources generating the ac voltage averaged over one cycle of the switching frequency. The model does not generate harmonics, but it does reflect the dynamics of the interaction between the power system and the control system.
- **BSS:** Bidirectional dc/ac converters and lithium batteries with maximum output power of 100 kWh (0.02 pu) for BSS<sub>1</sub> and 75 kWh (0.015 pu) for BSS<sub>2</sub> are used. The charging power for every BSS is 50 kW (0.01 pu). Buck-boost converters are used to charge the batteries when the system has enough generating capacity and to feed loads and respond to low RES power generation due to weather conditions, e.g. PV array power output variations are affected by sun shades.

DERs do not provide system frequency regulation. Therefore, for power-flow calculations within the NMPC algorithm, the DERs (except for the DEG) are considered as load nodes operating at their rated powers, assuming negative power

consumption. During grid-connected operation, the main grid performs voltage and frequency control. During autonomous operation, local microgrid generation controls voltage and frequency.

Since a centralized controller will be used, an advanced metering infrastructure (AMI) is required in the microgrid. Therefore, it is assumed that every load has a smart meter. The smart meter performs instantaneous voltage, current and power and energy measurements, and power quality data, and has communications capability. Smart meter data includes the unique meter identifier and measured data values [21].

The system operator can remotely connect and disconnect sources to any customer in order to control the power-flows in the microgrid, based on the information collected from the smart meters. Smart meters collect data from the end consumers and transmit this information through the local area network to a data collector, which transmits it to the DMS. This process usually is executed every 15 minutes or as frequently as programmed by the DMS.

### III. CONTROLLER DESIGN

#### A. Nonlinear Model Predictive Control

NMPC is a variant of model predictive control (MPC) that is characterized by the use of nonlinear system models to predict and optimize the future system behavior [22]. Additionally, the method allows incorporating nonlinear constraints on the state and the control variables, and the use of cost functions different from the classic quadratic form since the use of finite-time horizon for optimization. A generalized nonlinear discrete-time model of the system is defined as:

$$\mathbf{x}_{k+1} = f(\mathbf{x}_k, \mathbf{u}_k) \quad (1)$$

where  $f : \mathbb{R}^n \times \mathbb{U}^m \rightarrow \mathbb{R}^n$  assigns  $\mathbf{x}_{k+1} \in \mathbb{R}^n$  at the next time instant to each pair of state vector  $\mathbf{x}_k \in \mathbb{R}^n$  and control signal vector  $\mathbf{u}_k \in \mathbb{U}^m$ .

The main objective of MPC is to control the state  $\mathbf{x}_k$  of the system towards a reference trajectory  $\mathbf{r}_k$  and to keep the system state close to this reference [23]. Without loss of generality, the reference trajectory is considered constant in the prediction horizon, and an equilibrium point of the closed-loop system is defined by:

$$\mathbf{x}_{k+1}^* = f(\mathbf{x}_k, \mu(\mathbf{x}_k)) \quad (2)$$

where  $\mu(\cdot) : \mathbb{R}^n \rightarrow \mathbb{U}^m$  is the closed-loop control law obtained with the NMPC algorithm.

A set of finite control sequences is obtained after the optimization process:  $\mathbf{u}_0, \mathbf{u}_1, \dots, \mathbf{u}_{N-1}$  for  $N \in \mathbb{N}$  being the optimization horizon. Therefore, given an initial value  $\mathbf{x}_0 \in \mathbb{R}^n$  and a control sequence  $\mathbf{u}(\cdot) \in \mathbb{U}^K$  a trajectory of Eq. (1) is obtained iteratively via:

$${}^u\mathbf{x}_{k+1} = f({}^u\mathbf{x}_k, \mathbf{u}_k) \quad (3)$$

where  ${}^u\mathbf{x}_k$  is the predicted state of the system when the optimized control sequence  $\mathbf{u}(\cdot)$  is applied.

One of the strengths of MPC is its ability to manage constraints in its structure. Therefore, it is necessary to define valid numerical sets for the states of the system,  $\mathbf{x} \in \mathbb{X}_{x_{min}}^{x_{max}} \in \mathbb{R}^n$  and the control signals,  $\mathbf{u} \in \mathbb{U}_{u_{min}}^{u_{max}} \in \mathbb{R}^m$ .

### B. NMPC Design

The following equations were developed for designing the centralized NMPC strategy. The system states for the islanded section (left side feeder) of the distribution system of Fig. 1 are defined as:

$$\mathbf{x} = \begin{bmatrix} \mathbf{x}_1 \\ \mathbf{x}_2 \end{bmatrix} \quad \mathbf{x}_1 \in \mathbb{R}^{10} \quad \mathbf{x}_1 = [V_1 \dots V_{10}]^T \quad (4)$$

$$\mathbf{x}_2 \in \mathbb{R}^{10} \quad \mathbf{x}_2 = [\delta_1 \dots \delta_{10}]^T$$

where  $V_i$  and  $\delta_i$  are node's voltage and angle of the bus  $i$ .

Additionally, more variables and vectors are needed for the controller formulation, such as: power at the nodes  $S_i = P_{L_i} + jQ_{L_i}$ , admittance matrix  $\mathbf{Y}$ , and power generated by the DERs units,  $P_{DER_i}$ :

$$\mathbf{Y} = [Y_{ij}] \quad (5)$$

$$\mathbf{S} = \begin{bmatrix} \mathbf{P}_{load} \\ \mathbf{Q}_{load} \end{bmatrix} \quad \mathbf{P}_{load} \in \mathbb{R}^{10} \quad \mathbf{P}_{load} = [P_{L_i}]^T \quad (6)$$

$$\mathbf{Q}_{load} \in \mathbb{R}^{10} \quad \mathbf{Q}_{load} = [Q_{L_i}]^T$$

$$\mathbf{P}_{DERs} = [P_{DER_i}]^T \quad i = 1, \dots, 8 \quad \left\{ \begin{array}{ll} i = 1 & P_{DE} \\ i = 2 & P_{WT} \\ i = 3 & P_{PV_1} \\ i = 4 & P_{PV_2} \\ i = 5 & P_{PV_3} \\ i = 6 & P_{PV_4} \\ i = 7 & P_{BSS_1} \\ i = 8 & P_{BSS_2} \end{array} \right. \quad (7)$$

$$S_i = V_i \sum_{m=1}^N (Y_{im} V_i)^* \quad (8)$$

Eq. (8) is solved iteratively through the NR power-flow algorithm [24], with prior knowledge of  $P_{DER_i}$ ,  $i = 2, 3, \dots, 8$ , and current load consumption of every power system node. The power generated by the DEG ( $P_{DE}$ ) is estimated in a prediction horizon of length  $N$ . One important modification to the power flow equation is the inclusion of the reactive power consumed by the WTG at Bus 7, which is calculated as follows [25]:

$$Q_{WT} = -\frac{V_7^2}{z_p} + \frac{-V_7^2 + \sqrt{V_7^4 - 4P_7 z^2}}{2z} \quad (9)$$

$$z = z_1 + z_2; \quad z_p = \frac{z_c z_m}{z_c - z_m}$$

where the negative sign of Eq. (9) represents reactive power consumption of the WTG induction generator from the network;  $z_m$ ,  $z_c$ ,  $z_1$  and  $z_2$  represent the excitation reactance, reactance of the capacitor banks installed at the terminal of the induction generator and the stator and rotor reactance, respectively.

The objectives of this control strategy are:

- to manage the batteries energy;

- to disconnect low priority loads when the predicted load demand is greater than the generation capacity of the microgrid;
- to preserve microgrid stability and to keep the voltage magnitude with a maximum variation of  $\pm 5\%$ .

The centralized NMPC is implemented in the microgrid centralized-controller (MGCC). A control vector  $\mathbf{u}$  for managing loads connection and disconnection, as well as batteries charging and discharging modes is defined in Eq. (10). Table I shows the relationship between each bit of the control vector and its corresponding load controller for switching purposes, *i.e.* for  $u_i = 1 \rightarrow L_i$  load is connected, and for  $u_i = 0 \rightarrow L_i$  load is disconnected.

$$\mathbf{u} = [u_i] \quad i = 1, \dots, 13 \quad u_i \text{ is a binary signal} \quad (10)$$

TABLE I  
CONTROL VECTOR CORRESPONDENCE WITH LOADS AND BSS

Control bit	Load	Observations	Priority
$u_1$	$L_1^* = \{L_1 \cup L_2\}$	Variable loads	High
$u_2$	$L_3 \cup L_4$	Constant loads	Low
$u_3$	$L_5$	Constant load	Low
$u_4$	$L_6$	Variable load	Low
$u_5$	$L_7$	Variable load	High
$u_6$	$L_8$	Constant load	High
$u_7$	$L_9$	Variable load	Low
$u_8$	$L_{10}$	Constant load	Low
$u_9$	$L_{11}$	Constant load	Low
$u_{10}$	$BSS_1$	Charge mode	-
$u_{11}$	$BSS_1$	Discharge mode	-
$u_{12}$	$BSS_2$	Charge mode	-
$u_{13}$	$BSS_2$	Discharge mode	-

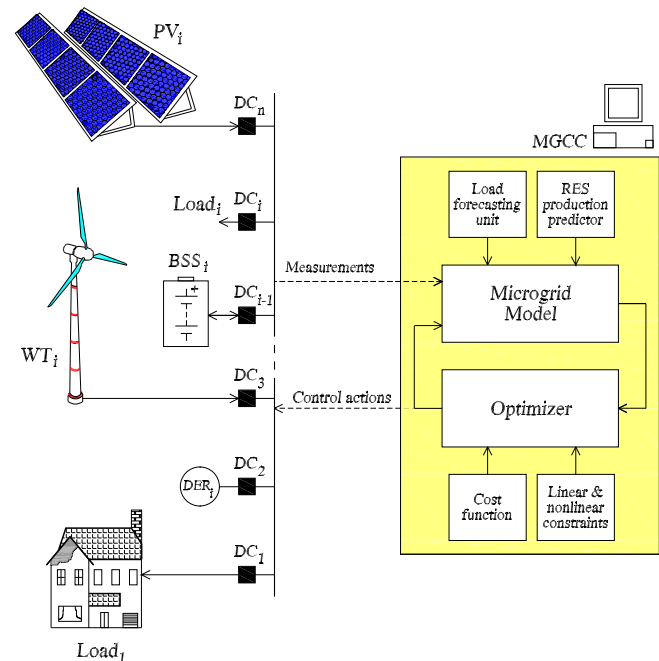


Fig. 3. NMPC architecture for a centralized load shedding strategy

An important requirement in the design of NMPC is the availability of a model for predicting the output variable. In our case, predicted values of  $P_{DE}$  are needed to optimally decide whether a load shedding must be performed or not. Once all loads to be shed are selected by the load shedding algorithm, trip commands are sent from the MGCC to the proper loads. Fig. 3 shows the controller architecture for integrating the NMPC in the MGCC.

The NR power-flow algorithm is used for predicting the microgrid system states  $\mathbf{x} \in \mathbb{R}^{20}$ , which are used to calculate  $P_{DE}$  in a prediction horizon  $N$ . The control vector  $\mathbf{u}$  commands loads connection and disconnection, as well as batteries charge and discharge processes within the NR algorithm. An initial data set  $\mathbb{Z}_k = [\mathbf{P}_{DG}(k)^T \quad \mathbf{P}_{load}(k)^T \quad \mathbf{SOC}^T]^T$  composed by the active power generated by every DER, load demand, and the batteries' SOC is needed before the execution of the NR power flow algorithm. The data set  $\mathbb{Z}_k$  does not consider load variations within the prediction horizon. This fact is considered, and two approaches were tested for the initial iterative load values of the NR algorithm in order to predict the  $P_{DE}$ :

- 1) Take the load measurements and keep them as constants during the prediction horizon  $N$ ;
- 2) Use a load predictor based on ANNs. Twenty load profiles from different days of the week for every variable load in the microgrid were used for training a three-layer ANN. The load predictor receives the load measurements and the hour of the day as inputs, and provides the load prediction for the upcoming 45 minutes, as shown in Fig. 4.

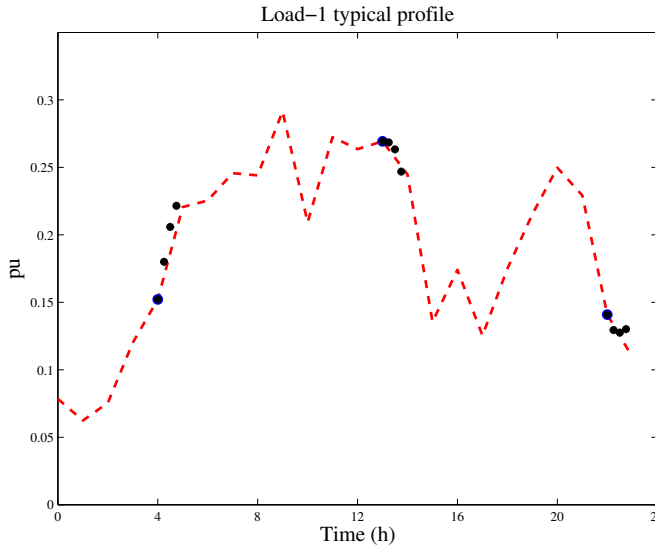


Fig. 4. Load-1 prediction using ANN

The encircled first dot shown in Fig. 4 at 4:00 AM represents the load measurement and the remaining three dots represent the predictions made by the ANN predictor every 15 minutes. Three more predictions can be observed in the figure at 13:00 PM and 22:00 PM. The dashed line in Fig. 4 represents the true load demand value.

Another approach for predicting the  $P_{DE}$  was developed with an ARX model through a data-based modeling approach using ANFIS. Twenty different generation profiles of the DEG for different days of the week were used as training set for the ANFIS. Fig. 5 shows the ARX-ANFIS model configuration. This modeling procedure does not imply an NR power-flow calculation, which reduces the computing time of the control algorithm.

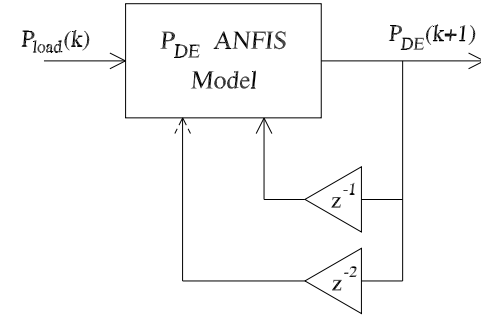


Fig. 5. ARX-ANFIS model for predicting  $P_{DE}$

### C. NMPC Algorithm

Since the voltage magnitude of the microgrid is to be kept within a  $\pm 5\%$  range of variation, the static voltage stability index  $L$ , presented in [25] is used for defining a secure range of operation of the DEG. Considering the average generation values of the DERs:  $P_{WT} = 0.15$ ,  $\sum_{i=1}^4 P_{PV_i} = 0.049$  and  $\sum_{i=1}^2 P_{BSS_i} = 0.035$  in discharge mode and  $\sum_{i=1}^2 P_{BSS_i} = -0.02$  in charge mode; and that the voltage magnitude limits are  $0.95 \leq |V| \leq 1.05$ , an optimization procedure in which a sweep of the values of  $P_L$ ,  $Q_L$ , and  $|V|$  within allowable ranges was performed as follows:

$$\begin{aligned}
 & \text{minimize} && |1 - L| \\
 & \text{subject to} && \\
 & P_{DE} + P_{WT} + \sum_{i=1}^4 P_{PV_i} \pm \sum_{j=1}^2 P_{BSS_j} = P_L + P_{loss} \\
 & L_{i+1} = 4 \frac{(X_{eq} P_L - R_{eq} Q_L)^2 + (X_{eq} Q_L + R_{eq} P_L) V_i^2}{V_i^4} < 1 \\
 & 0 < P_L < P_{max} \\
 & 0 < Q_L < Q_{min} \\
 & 0.95 \leq |V| \leq 1.05
 \end{aligned} \tag{11}$$

where  $X_{eq}$  and  $R_{eq}$  are the equivalent reactance and resistance of the microgrid, respectively. The secure range of operation of  $P_{DE}$ , estimated by the optimization process in (11) is:

$$P_{DE} \leq P_{DE}^+ = 0.2 \tag{12}$$

Therefore, the cost function  $J$  to be used in the optimization algorithm will operate the master generation unit of the microgrid, the diesel engine, in a range of power generation that guarantees voltage stability. The cost function is defined as follows:

$$J(\mathbf{x}_k) = (P_{DE}(\mathbf{x}_k) - r)^2 \quad (13)$$

where  $P_{DE}(\mathbf{x}_k)$  is calculated through the NR algorithm as it was described in the previous section, or by the use of the ARX-ANFIS model. The value of  $r$  is selected to be less than  $P_{DE}^+$ .

A list of steps for implementing the NMPC algorithm described is shown in Algorithm 1.

The control vector  $\mathbf{u}$  of Algorithm 1, for the particular case of the proposed NMPC algorithm is restricted to be binary. Problems of this type are generally named mixed-integer nonlinear programming (MINLP) problems. The mixed-integer linear, quadratic and nonlinear programming package of TOMLAB for MATLAB was used for solving the optimal control problem. To solve the MINLP problem, TOMLAB implements a branch-and-bound algorithm searching a tree whose nodes correspond to nonlinearly constrained continuous optimization problems. The continuous problems are solved using sequential quadratic programming. The method avoids the use of penalty functions. Global convergence is enforced through the use of a trust region and a filter that accepts a trial point whenever the objective or the constraint violation is improved compared to all previous iterations.

**Algorithm 1:** NMPC algorithm for automated load shedding and BSS management

- 1: Define a DE power generation reference  $r < P_{DE}^+$
  - 2: Take system measurements:
- $$\mathbb{Z}_k = [\mathbf{P}_{DG}(k)^T \quad \mathbf{P}_{load}(k)^T \quad \mathbf{SOC}^T]^T$$
- 3: Solve the following optimal control problem:

minimize

$$J_N = \sum_{k=0}^{N_p-1} ({}^u P_{DE_k}(\mathbb{Z}_k, \mathbf{x}_k, \mathbf{u}_k) - r)^2$$

subject to

$$\begin{aligned} {}^u P_{DE_{k+1}} &= f({}^u P_{DE_k}(\mathbb{Z}_k, \mathbf{x}_k, \mathbf{u}_k), \mathbf{u}_{k+1}) \\ P_L(k) + P_{loss} &= \sum_{i=2}^8 P_{DER_i}(k) + P_{DE_k} \end{aligned}$$

and constrained to

- $P_{DE_{min}} = 0.05 < P_{DE} < P_{DE}^+ = 0.2$
- $L_1, L_7$  and  $L_8$  always have to be connected (high priority loads);
- At least one of the following loads has to be connected:  $L_3, L_5$  or  $L_{11}$  (low priority loads);
- At least one of the following loads has to be connected:  $L_6, L_9$  or  $L_{10}$  (low priority loads);
- $\{\forall t : P_{DE} < r \cap SOC < 100\%\} \rightarrow$  batteries go into charging mode;
- $\{\forall t : P_{DE} > r \cap SOC > 30\%\} \rightarrow$  batteries go into discharge mode;
- The minimum load to be shed is 10% of the actual connected load.

- 4: Define the control law  $\mu(\mathbb{Z}_k) = \mathbf{u}^*(1)$

#### IV. SIMULATION RESULTS

A 24-hour simulation was performed for testing the proposed controller. Variable profiles for wind velocity and solar radiation were used during the simulation, as shown in Fig. 6. The microgrid starts operating in grid-connected mode and at 2:00 AM, an islanding operation is simulated in the left side feeder. The right side feeder is not considered in this case, since  $S_c$  is open (see Fig. 1).

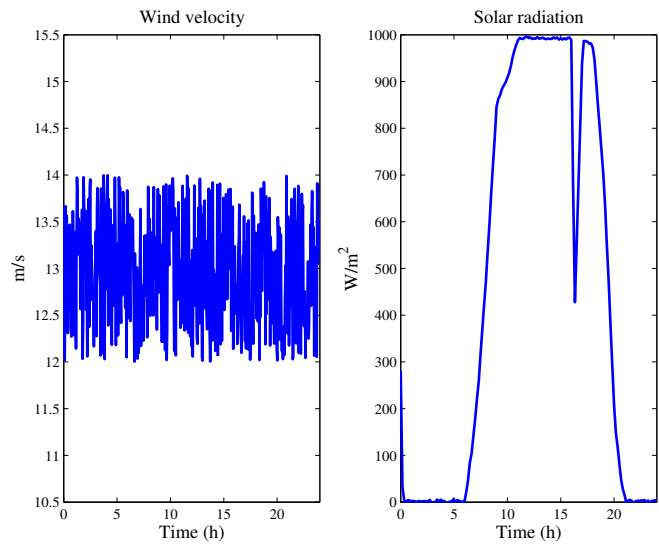


Fig. 6. Profiles of wind velocity and solar radiation used in the simulation

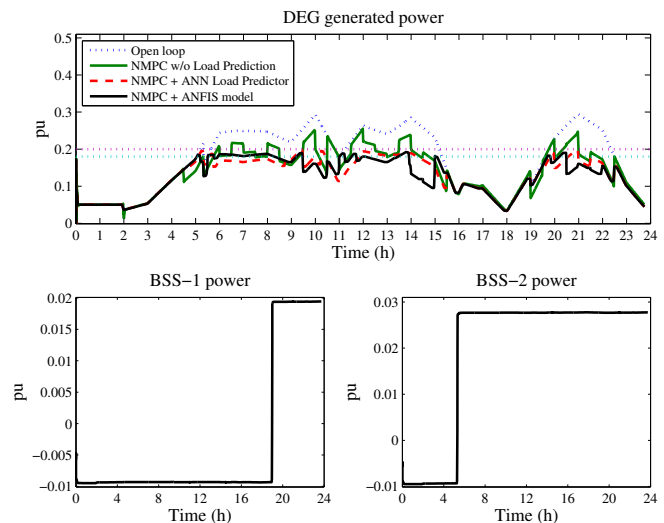


Fig. 7. Performance comparison of the NMPC with different model approaches (batteries in the charge-discharge mode)

The MGCC is monitoring the microgrid all the time for alerting an islanding event. Islanding detection is out of the scope of this paper; interested readers are referred to [26] for available islanding detection techniques. Once the islanding condition is confirmed by an islanding detection algorithm, the NMPC starts processing data every 15 minutes, except when  $P_{DE} > 1.1 \times r$ , which means that the DE operates near its generation limits. In this case, the algorithm evaluates all the variables in order to calculate the amount of load to shed until the next scheduled calculation loop.

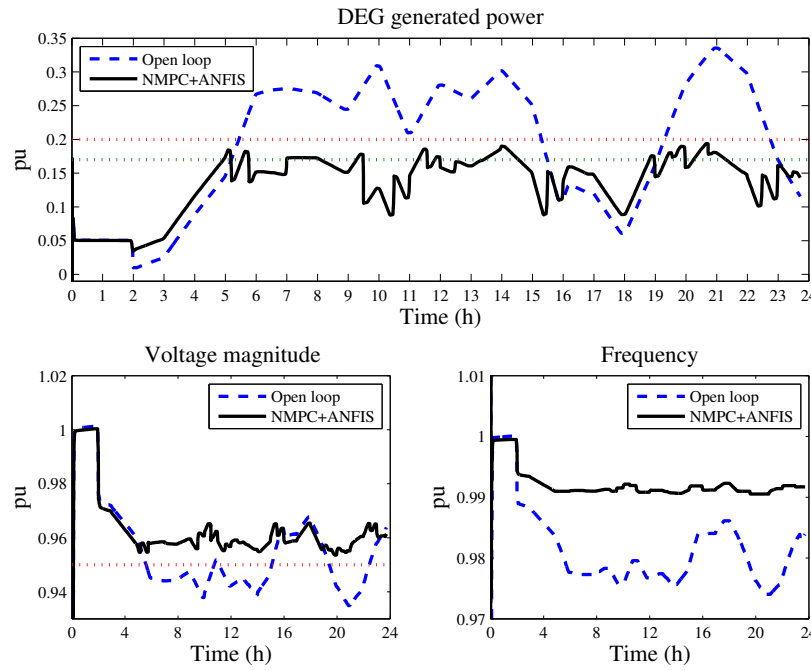


Fig. 8.  $P_{DE}$  output signal when the load shedding NMPC strategy is used (batteries in the switching mode)

Fig. 7 shows a performance comparison of the NMPC algorithm operating the microgrid. The three different techniques for predicting the  $P_{DE}$  output, detailed in Section III.B, are used for an optimization horizon  $N = 2$  and a sampling time of 15 minutes. The approach that keeps the loads measurements constant for the power-flow calculation in the prediction horizon offers the worst results. The  $P_{DE}$  overpasses the safe limit of generation. On the other hand, the use of the ANN load predictor in the power-flow calculation shows much better results, and the generation profile of the DEG never violates the 0.2 pu limit. Finally, the ARX-ANFIS model offers the best result, since the generation profile is kept much closer to the selected reference  $r = 0.18$ , which is the same for all the cases. For these tests, no battery management strategy is implemented. Batteries are in a charge-discharge mode, and are assumed to be available when needed, as shown in Fig. 7.

Figs. 8 and 9 provide additional information on the NMPC algorithm performance. These figures show microgrid voltage and frequency behavior, and loads and batteries switching due to the NMPC optimal decisions. The voltage magnitude keeps within the  $\pm 5\%$  band when the microgrid is islanded, which is not the case when no control action is performed (see Fig. 8). Additionally, the constraints included in the NMPC algorithm are not violated. High priority loads  $L_1^*$ ,  $L_7$  and  $L_8$  were not disconnected, and at least one load of every low priority load group kept connected, as it was programmed in the NMPC algorithm (see Fig. 9). Furthermore, batteries charge at the off-peak times, when there is availability of power from the generation units. Batteries go into discharge mode (delivering power to the grid) when there is a power deficit due to peak consumption (Fig. 9). The inclusion of load shedding and battery management in the NMPC algorithm (Figs. 8 and 9)

improves its performance with respect to the one showed in Fig. 7 where an open-loop batteries strategy was tested.

Based on experiments, some algorithm limitations are identified:

- Model accuracy directly affects the controller's performance;
- Does not include economic dispatch (future work);
- Assumes knowledge of the power generated by the RES in every time step;
- Does not consider communication delays (perfect telecommunication network);
- The charging and discharging rates of the batteries were not considered, since the energy coming from the batteries were guaranteed to be present for at least one sampling period of the NMPC calculation (15 minutes).

## V. CONCLUSIONS

An optimal predictive control strategy for energy management of the batteries and load shedding purposes has been designed and tested in an isolated microgrid with DERs. This algorithm is implemented in the MGCC. Significant performance improvement has been achieved with the use of this proposed controller over simulations performed without it, since it allows to avoid power unbalances through an optimal load shedding strategy and to keep the voltage magnitude within safe limits, thus increasing the performance and the security of the islanded operation of the microgrid.

Good energy management in an isolated microgrid should first ensure continuous supply to critical loads. Thereafter, other targets could be set, such as maximizing efficiency, reducing operating costs and so on.

The comparison between the use of this algorithm and an open-loop system condition shows the benefits of the

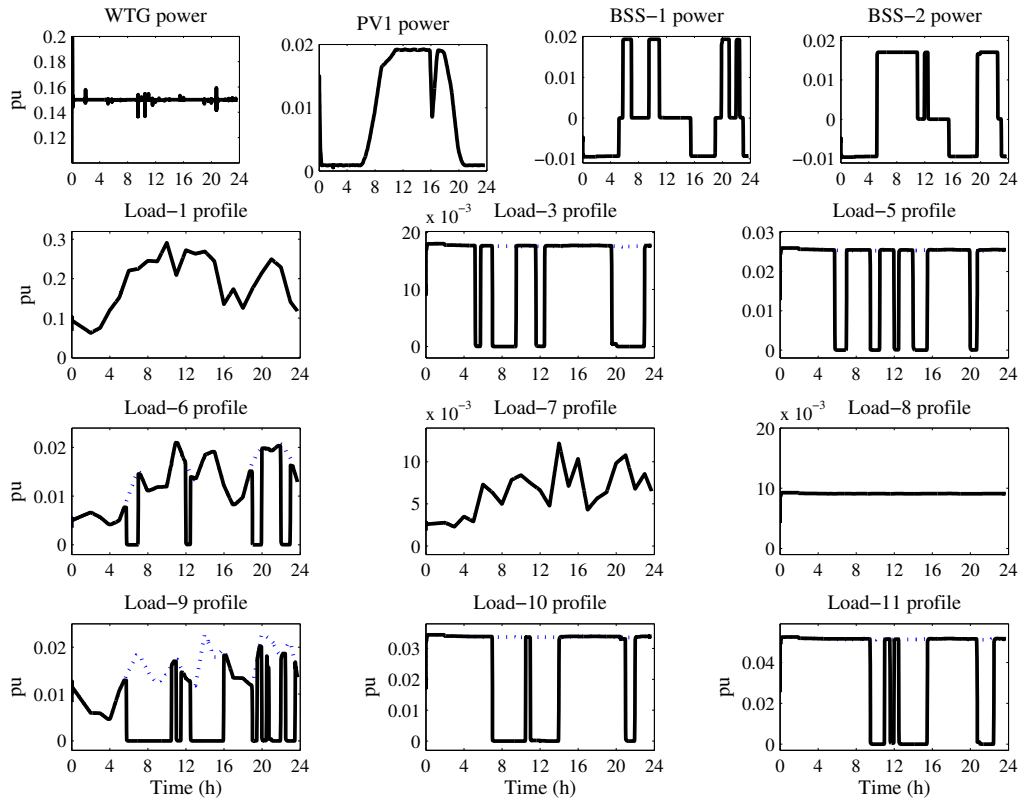


Fig. 9. Profiles of RES generated power and load power consumption

technique: the voltage magnitude remains stable and close to its normal operating value (1 pu), an load is served, except for the disconnection of some low priority loads when necessary. In the discharge mode the batteries send active power to the grid, while in the charge mode the batteries consume active power to charge.

When the microgrid goes to islanded mode, the diesel engine generator supplies all the power demand that is not supplied by the other DERs. Due to the rated power limitations of the DEG, significant load shedding was necessary for high load condition in the system.

## REFERENCES

- [1] F. Kennel, D. Gorges, and S. Liu, "Energy management for smart grids with electric vehicles based on hierarchical MPC," *IEEE Transactions on Industrial Informatics*, vol. 9, pp. 1528–1537, Aug 2013.
- [2] M. Kabir, Y. Mishra, G. Ledwich, Z. Dong, and K. Wong, "Coordinated control of grid-connected photovoltaic reactive power and battery energy storage systems to improve the voltage profile of a residential distribution feeder," *IEEE Transactions on Industrial Informatics*, vol. 10, pp. 967–977, May 2014.
- [3] E. Planas, A. G. de Muro, J. Andreu, I. Kortabarria, and I. M. de Alegra, "General aspects, hierarchical controls and droop methods in microgrids: A review," *Renewable and Sustainable Energy Reviews*, vol. 17, pp. 147–159, 2013.
- [4] P. Garcia, C. Garcia, L. Fernandez, F. Llorens, and F. Jurado, "ANFIS-based control of a grid-connected hybrid system integrating renewable energies, hydrogen and batteries," *IEEE Transactions on Industrial Informatics*, vol. 10, pp. 1107–1117, May 2014.
- [5] Y. Zhou, H. Held, W. Klein, K. Majewski, R. Speh, P. E. Stelzig, and C. Wincheringer, "SoftGrid: A green field approach of future smart grid," in *Proceeding of the 2nd International Conference on Smart Grids and Green IT Systems*, pp. 5–11, May 2013.
- [6] A. Tsikalakis and N. Hatziargyriou, "Centralized control for optimizing microgrids operation," *IEEE Transactions on Energy Conversion*, vol. 23, pp. 241–248, March 2008.
- [7] S. Conti, R. Nicolosi, S. A. Rizzo, and H. Zeineldin, "Optimal dispatching of distributed generators and storage systems for MV islanded microgrids," *IEEE Transactions on Power Delivery*, vol. 27, no. 3, pp. 1243–1251, 2012.
- [8] A. Venkat, I. Hiskens, J. Rawlings, and S. Wright, "Distributed MPC strategies with application to power system automatic generation control," *IEEE Transactions on Control Systems Technology*, vol. 16, pp. 1192–1206, Nov 2008.
- [9] F. Drfler, John-Simpson-Porco, and F. Bullo, "Breaking the hierarchy: Distributed control & economic optimality in microgrids," *arXiv preprint arXiv:1401.1767*, 2014.
- [10] S. Anand, B. G. Fernandes, and M. Guerrero, "Distributed control to ensure proportional load sharing and improve voltage regulation in low-voltage DC microgrids," *IEEE Transactions on Power Electronics*, vol. 28, pp. 1900–1913, April 2013.
- [11] L. I. Minchala-Avila, L. E. Garza-Castañón, A. Vargas-Martínez, and Y. M. Zhang, "A review of optimal control techniques applied to the energy management and control of microgrids," *Procedia Computer Science*, vol. 52, pp. 780–787, 2015.
- [12] Z. Styczynski, A. Orths, K. Rudion, A. Lebioda, and O. Ruhle, "Benchmark for an electric distribution system with dispersed energy resources," in *Transmission and Distribution Conference and Exhibition*, pp. 314–320, 2006.
- [13] B. Mao, B. Zhang, J. Wang, Y. Chen, X. Zheng, Y. Gao, B. Wu, and Y. Liu, "Dynamic modelling for distribution networks containing dispersed generations and energy storage devices," in *International Conference on Power System Technology (POWERCON)*, pp. 1–6, 2010.
- [14] S. Tomohiko, T. Shen, Y. Sun, and J. Xu, "Modeling and control of a benchmark micro grid with vehicle-to-grid smart connection," in *the 30th Chinese Control Conference (CCC)*, pp. 6121–6126, 2011.
- [15] "IEEE application guide for IEEE std 1547, IEEE standard for interconnecting distributed resources with electric power systems," *IEEE Std 1547.2-2008*, pp. 1–207, 2009.
- [16] K. Rudion, A. Orths, Z. Styczynski, and K. Strunz, "Design of benchmark of medium voltage distribution network for investigation of DG

- integration," in *Power Engineering Society General Meeting*, pp. 6–12, 2006.
- [17] "IEEE guide for design, operation, and integration of distributed resource island systems with electric power systems," *IEEE Std 1547.4-2011*, pp. 1–54, July 2011.
- [18] A. Vargas-Martínez, L. I. Minchala-Avila, Y. M. Zhang, L. E. Garza-Castañón, and P. Acosta-Santana, "Fault-tolerant controller design for a master generation unit in an isolated hybrid wind-diesel power system," *International Journal of Robust and Nonlinear Control*, vol. 25, no. 5, pp. 761–772, 2015.
- [19] A. Vargas-Martínez, L. I. Minchala-Avila, Y. M. Zhang, L. E. Garza-Castañón, and H. Badihi, "Hybrid adaptive fault-tolerant control algorithms for voltage and frequency regulation of an islanded microgrid," *International Transactions on Electrical Energy Systems*, vol. 25, no. 5, pp. 827–844, 2015.
- [20] L. Minchala-Avila, A. Vargas-Martínez, Y. M. Zhang, and L. Garza-Castañón, "A model predictive control approach for integrating a master generation unit in a microgrid," in *Conference on Control and Fault-Tolerant Systems (SysTol)*, pp. 674–679, Oct 2013.
- [21] J. Zheng, D. Gao, and L. Lin, "Smart meters in smart grid: An overview," in *Green Technologies Conference*, pp. 57–64, April 2013.
- [22] L. Grüne and J. Pannek, *Nonlinear Model Predictive Control: Theory and Algorithms*. Springer, 2011.
- [23] J. Maciejowski, *Predictive Control with Constraints*. Prentice-Hall, 2002.
- [24] J. Glover, M. Sarma, and T. Overbye, *Power System Analysis and Design*. Cengage Learning, 2011.
- [25] H. Chen, J. Chen, D. Shi, and X. Duan, "Power flow study and voltage stability analysis for distribution systems with distributed generation," in *2006 IEEE Power Engineering Society General Meeting*, pp. 1–8, 2006.
- [26] R. Kunte and W. Gao, "Comparison and review of islanding detection techniques for distributed energy resources," in *40th North American Power Symposium*, pp. 1–8, Sept 2008.

## APPENDIX: BENCHMARK MODEL PARAMETERS

TABLE II  
LOAD PARAMETERS OF THE BENCHMARK MICROGRID MODEL

Load No.	Load Type	$P_{max}$ (pu)	$Q_{max}$ (pu)
1	Industrial	0.15000	0.03100
2	Residential	0.05000	0.01000
3	Residential	0.00276	0.00069
4	Industrial	0.00224	0.00139
5	Residential	0.00432	0.00108
6	Residential	0.00725	0.00182
7	Residential	0.00550	0.00138
8	Industrial	0.00077	0.00048
9	Residential	0.00588	0.00147
10	Industrial	0.00574	0.00356
11	Industrial	0.00068	0.00042
12	Household	0.00477	0.00120
13	Household	0.00331	0.00083
14	Residential	0.15000	0.03000
15	Industrial	0.05000	0.01700
16	Industrial	0.00032	0.00020
17	Industrial	0.00330	0.00020
18	Residential	0.00207	0.00052



**Luis I. Minchala-Avila** (M'05) received his B.S.E.E. degree in 2006 from the Salesian Polytechnic University in Cuenca, Ecuador, and his Ms.C and Ph.D. degrees from Instituto Tecnológico y de Estudios Superiores de Monterrey in Monterrey, México, in 2011 and 2014, respectively. During summer 2012 to summer 2013 he was a visiting scholar in Concordia University in Montreal, Canada. From 2015 Dr. Minchala is a full time researcher with the department of electrical, electronic and telecommunications engineering at Universidad de Cuenca. His research interests are model-based control algorithms, process optimization and automation, microgrids control, and systems modeling.

TABLE III  
POWER LINE PARAMETERS OF THE BENCHMARK MICROGRID MODEL

From Node	To Node	$R$ ( $\frac{\Omega}{Km}$ )	$X$ ( $\frac{\Omega}{Km}$ )	$C$ ( $\frac{nF}{Km}$ )	$L$ (Km)
1	2	0.579	0.367	158.88	2.82
2	3	0.164	0.113	6608	4.42
3	4	0.262	0.121	6480	0.61
4	5	0.354	0.129	4560	0.56
5	6	0.336	0.126	5488	1.54
6	7	0.256	0.13	3760	0.24
7	8	0.294	0.123	5600	1.67
8	9	0.339	0.13	4368	0.32
9	10	0.399	0.133	4832	0.77
10	11	0.367	0.133	4560	0.33
11	4	0.423	0.134	4960	0.49
3	8	0.172	0.115	6576	1.3
12	13	0.337	0.358	162.88	4.89
13	14	0.202	0.122	4784	2.99



**Luis Garza-Castañón** (M'08) received his B.S.E.E. degree in 1986 from the Tecnológico de Monterrey in Monterrey, NL, México and his Ph.D. degree in 2001 from the same university. From 1988 until 1998, Dr. Garza-Castañón worked as an automation and control engineer at Altos Hornos de México and Inmagusa Company, both located in Monclova, Coah., Mexico. From 1999 to 2003 served as part-time professor on the Physics Department at the Tecnológico de Monterrey. In 2004 he joined the Mechatronics and Automation Department at the Tecnológico de Monterrey, where he is currently an associate professor and researcher. He has authored and coauthored more than 80 technical papers and book chapters. His main research interests are in fault detection and diagnosis, fault tolerant control and leak detection in water networks. Dr. Garza-Castañón is an IEEE member.



**Youmin Zhang** (SM'07) received the B.S., M.S., and Ph.D. degrees with a specialization in automatic controls from Northwestern Polytechnical University, Xian, China, in 1983, 1986, and 1995, respectively. Dr. Zhang is currently a Professor with the Department of Mechanical and Industrial Engineering and the Concordia Institute of Aerospace Design and Innovation, Concordia University, Montreal, Quebec, Canada. His current research interests include condition monitoring, health management, fault diagnosis, and fault-tolerant (flight) control systems, cooperative guidance, navigation, and control (GNC) and remote sensing of unmanned aerial/space/surface vehicles and their applications, dynamic systems modeling, estimation, identification, advanced control techniques and signal processing techniques for diagnosis, prognosis, and health management of safety-critical systems, renewable energy systems and smart grids, and manufacturing processes. He has authored four books, over 380 journal and conference papers, and book chapters.



**Héctor J. Altuve Ferrer** (SM'95, Fellow'15) received his B.S.E.E. degree in 1969 from the Central University of Las Villas in Santa Clara, Cuba, and his Ph.D. degree in 1981 from Kiev Polytechnic Institute in Kiev, Ukraine. From 1969 until 1993, Dr. Altuve served on the faculty of the Electrical Engineering School at the Central University of Las Villas. From 1993 to 2000, he served as professor of the Graduate Doctoral Program in the Mechanical and Electrical Engineering School at the Autonomous University of Nuevo Len in Monterrey, Mexico. In 1999 through 2000, he was the Schweitzer Visiting Professor in the Department of Electrical and Computer Engineering at Washington State University. Dr. Altuve joined Schweitzer Engineering Laboratories, Inc. (SEL) in January 2001, where he is currently a distinguished engineer and dean of SEL University. He has authored and coauthored more than 100 technical papers and several books and holds four patents. His main research interests are in power system protection, control, and monitoring. Dr. Altuve is an IEEE fellow.